JOURNAL OF GEOPHYSICAL RESEARCH, VOL. 95, NO. A4, PAGES 3819–3828, APRIL 1, 1990

Current Sheet Thickness in the Near-Earth Plasma Sheet During Substorm Growth Phase

V. A. SERGEEV,[1] P. TANSKANEN,[2] K. MURSULA,[2] A. KORTH,[3] AND R. C. ELPHIC[4]

Magnetic field measurements made in the Earth's tail region during the growth phases of substorms on May 23, 1979, by GEOS 2 and ISEE 1, and on June 23, 1979, by GEOS 2 and IMP-J, were used to model the magnetic configuration in the location conjugate to the Scandinavian riometer network. Toward the end of the growth phase the time variation of the magnetic configuration explains about 80% of the equatorward expansion of the central part of the auroral oval. Assuming the origin of the observed equatorward moving band of energetic electron precipitation into the ionosphere to be caused by pitch angle scattering in the equatorial current sheet, we inferred the half thickness of the current sheet at $r \approx 9\ R_E$ as thin as $0.1\ R_E$ near the end of the growth phase. Combined with the modeled evolution of the magnetic configuration, this mechanism consistently explains the main features of the electron precipitation.

1. INTRODUCTION

The increase of the tail current and the overall stretching of the tail field lines together with the plasma sheet thinning are the most spectacular signatures of the substorm growth phase seen in the magnetotail [*Russell and McPherron*, 1973; *Nishida and Fujii*, 1976; *Fairfield et al.*, 1981]. According to the present view the half thickness (D) of the current sheet belongs to the small number of critical parameters controlling where and when the substorm expansion phase is first initiated [*Schindler and Birn*, 1982; *Büchner and Zelenyi*, 1987]. The direct estimate of this parameter requires a favorable location of more than one spacecraft. Such a study has appeared in the literature [*McPherron et al.*, 1987], where this parameter was found to decrease from about $5\ R_E$ to less than $1\ R_E$ at $r \approx 13\ R_E$ during the first 20 min of a very strong growth phase.

Another way to characterize the variations of the current sheet thickness is to use the observed time variations of the intensity gradient of energetic protons. *Buck et al.* [1973] employed this method to document the fast thinning of the layer containing the gyrocenters of energetic protons at $r \approx 8\ R_E$ toward the end of the growth phase of a strong substorm. Extremely small values of this layer ($0.1\ R_E$) just before the expansion onset have been explained as a signature of a very thin current layer. These results together with the findings of *Nishida and Fujii* [1976] indicate that, indeed, current sheet thickness may decrease drastically in the nightside part of plasma sheet at around $r \approx 8$–$10\ R_E$.

Here we shall describe another approach using the combination of simultaneous measurements made in the magnetotail as well as from the ground. The magnetic measurements in the tail are used to map the field lines from the magnetosphere to the ionosphere. On the other hand, the registration of precipitated energetic electrons, used as tracers of conditions in the equatorial portion of field lines, allows one to estimate the current sheet thickness in some flux tubes. To verify this approach, we shall further compare basic properties of the energetic particle precipitation inferred from our model calculations with those known from observations.

2. OBSERVATIONS

Two examples of substorms having relatively strong and isolated effects during the growth phase are studied here. Two spacecraft were in both cases fortunately located for comparison with observations from the ground network. GEOS 2, which was used in both events, was stationed at 37°E in a geosynchronous orbit, with its nominal conjugate point in northern Scandinavia.

The first event (see Figure 1) occurred on May 23, 1979, and was initiated by a smooth increase in the southward component of the interplanetary magnetic field (IMF) after 1800 UT (data not shown). The monotonous decrease of the vertical magnetic field component was observed at GEOS 2 and ISEE 1. Both spacecraft were located in the premidnight (22–23 MLT) sector. The increase of the tail-aligned field component $-B_x$ was seen at ISEE 1. During the growth phase an equatorward moving cosmic noise absorption (CNA) region was detected by the riometers at the Kevo and Ivalo stations. The expansion phase onset occurred at 2018 UT and was evidenced by the commencement of Pi 2 pulsations [*Lester et al.*, 1983; *Singer et al.*, 1983]. Unfortunately, the exact position of the current wedge could not be determined because of the lack of suitable magnetometer data. Concurrently, magnetic bays at mid-latitudes were observed (data not shown), as well as poleward expanding CNA and an increasing B_z component as registered by ISEE 1.

The second substorm event (see Figure 2), which occurred after 1930 UT on June 23, 1979, with an expansion phase onset at 2101 UT, has been presented in the paper by *Tanskanen et al.* [1987], who investigated the energy spectra, spatial pattern, and dynamics of the energetic electron precipitation region monitored by balloons and riometers. The riometer data and the GEOS 2 and IMP-J magnetic recordings are presented in Figure 2. The IMP-J spacecraft was located at that time in the southern tail lobe at $r \approx 33\ R_E$. In spite of the data gap the IMP-J measurements indicate a

[1]Institute of Physics, Leningrad State University, Leningrad.
[2]Department of Physics, University of Oulu, Oulu, Finland.
[3]Max-Planck-Institut für Aeronomie, Katlenburg-Lindau, Federal Republic of Germany.
[4]Los Alamos National Laboratory, Los Alamos, New Mexico.

Paper number 89JA01689.
0148-0227/90/89JA-01689$05.00

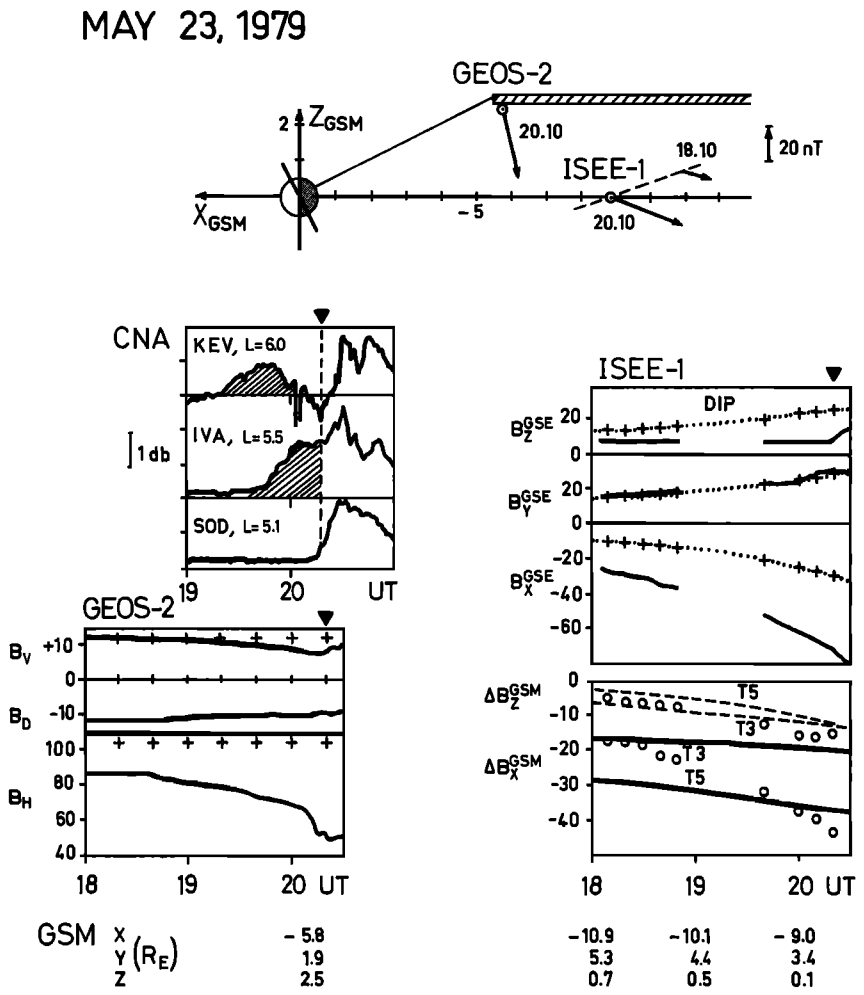

Fig. 1. A summary of observations during the growth phase of a substorm on May 23, 1979. The solid triangles indicate the onset of the substorm expansion phase at 2018 UT. (Bottom) The GSM coordinates (in R_E) of the two spacecraft for a few positions are given. (Top) The spacecraft configuration and the measured external (dipole field subtracted) magnetic field vectors in the GSM x-z plane are shown. The narrow hatched area indicates the approximate location of the current sheet. (Middle left) CNA amplitudes at the Finnish riometer chain are illustrated. (Bottom left) The V, D and H components of the magnetic field (in nanoteslas) measured by GEOS 2 are plotted. The dipole field components are shown here and elsewhere by plus signs. (Middle right) The GSE components of the magnetic field measured by ISEE 1 are shown. (Bottom right) The GSM x and z components of the external magnetic field are also illustrated. Circles give the values measured by ISEE 1, and curves indicate the values calculated along the ISEE 1 trajectory in two variants (K_p = 3 for line T3 and K_p = 5 for line T5) of the magnetospheric field model by *Tsyganenko* [1987].

substantial increase of the lobe field from 20 nT at 2000 UT up to 25 nT at 2100 UT.

The spatial patterns of the energetic electron precipitations for the two cases in our study are illustrated in Figure 3. The corrected geomagnetic coordinates of the points at 110 km height above the balloons and riometers are given in Table 1 together with the maximum CNA or auroral X ray intensity magnitudes and the universal times of onsets and peak precipitations. Typical examples of the inferred instantaneous positions of peak precipitation regions are shown in Figure 3. The solid lines connect a station (USH and S22 for May 23 and June 23, respectively), at the time of its maximum signal, with the expected position of the peak CNA region along the Ivalo-Kevo meridian at the same time. Then they are continued to the west using the peak absorption time of the Leirvogour station. The apparent equatorward drift speed of about 0.06°–0.07° min^{-1} at the Ivalo-Kevo meridian was estimated from a 18- to 20-min delay in the appearence of peak absorption over Kevo and Ivalo.

It is important to emphasize the similarity of the two growth phase events. They occurred in nearly the same MLT sector just prior to local midnight. They had comparable durations (1.5–2 hours) and similar intensities in the ground magnetic effects. In both cases the AU and AL indices reached a magnitude of 200–250 nT just before the expansion onset and the hourly averaged D_{st} values were −18 and −17 nT for the May 23 and June 23 events, respectively. The dynamical pressures of the solar wind [*King*, 1986] were also comparable. In both cases, no significant CNA effects were found over the extensive riometer network during the initial part of the growth phase, whereas the development of the CNA patterns toward the end of the growth phase was almost identical, though it appears to have moved further equatorward in the June 23 event (compare

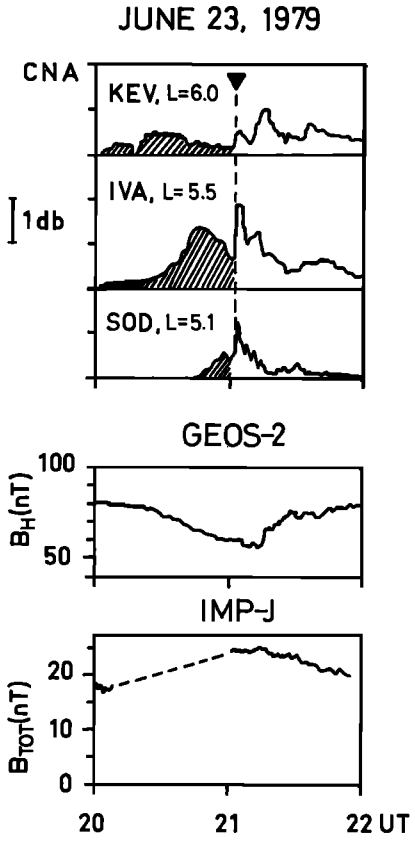

Fig. 2. A summary of observations during the growth phase of a substorm on June 23, 1979. The solid triangle indicates the onset of substorm expansion phase at 2101 UT. (Top) CNA amplitudes recorded by the Finnish riometers, (middle) the H component of the magnetic field measured by GEOS 2, and (bottom) the total magnetic field in the southern lobe measured by IMP-J at GSM x, y, z = [−26, −9, −17] R_E are illustrated.

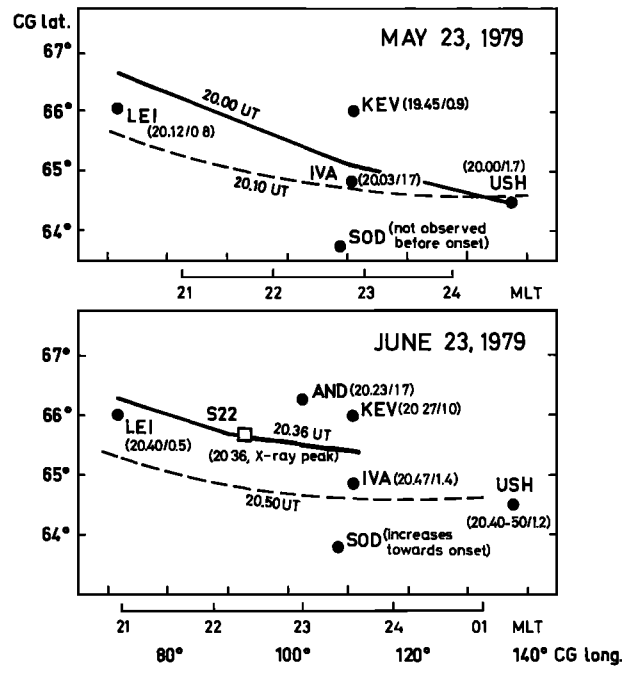

Fig. 3. The instantaneous configuration of the peak CNA region during the growth phases of the two substorms. Circles and rectangles stand for riometer and balloon positions, respectively. For each station the time and magnitude of the maximum signal (in decibels) are given, if observed (see also Table 1). The solid curves indicate the observed peak CNA fronts at the time of maximum signal at USH and S22, respectively. The dashed curves stand for calculated contours of the isotropic boundary for G = 800 nT km at later times.

Figures 1 and 2). The maximum CNA amplitude over Ivalo was reached in both events about 15 min before the expansion (see Table 1). Moreover, when the equatorward drifting CNA band was at the same latitude, the magnetic field observed at GEOS 2 was practically the same. When the CNA peak was over Kevo, the H component at GEOS 2 had the values of 74 nT and 76 nT for May 23 and June 23, respectively. When it was over Ivalo, the readings were 67 nT and 65 nT for May 23 and June 23, respectively. This implies close similarity in instantaneous magnetic configurations and energetic particle distributions in the near-Earth tail region at these particular times, as well as a very similar evolution of these patterns in time.

3. Signatures of the Energetic Electron Precipitation

Using the energetic particle precipitation to probe the magnetic field configuration in the nightside magnetosphere is based on the typical meridional distributions of trapped and precipitating particles shown in Figure 4. This schematic presentation shows the results of extensive measurements made on board low-altitude spacecraft [*Fritz*, 1970; *Imhof et al.*, 1979; *Lundblad et al.*, 1979]. Its main elements are independent of the particular substorm phase or activity level and can be summarized as follows: (1) the largest precipitation of radiation belt particles that is isotropic over the loss cone is seen in the outer portion of the radiation belt outside some boundary (here called the isotropic boundary, IB); (2) IB is rather sharp, its thickness only a few tenths of a degree of invariant latitude; (3) the instantaneous IB position depends on the particle rigidity G ($G = mV/e$; V is the total velocity of the particle) and is displaced toward the equator (earthward in the magnetotail) for particles of higher rigidity.

The results by *Lundblad et al.* [1979] and by *Rossberg* [1976] show that for energetic protons and for 40-keV electrons there is an equatorward displacement of IB during the growth phase of a substorm. In this scheme the intensity and dynamics of the energetic particle precipitation depend mainly on the IB position within the radiation belt. The simultaneous operation of some acceleration is not required, although it can not be excluded. According to this picture the IB position for energetic electrons corresponds to the region of their maximum precipitation. Thus it may be established at times when the intensity of the precipitation (monitored by X ray intensity or by CNA amplitude) reaches a maximum over a particular station during the equatorward drift of the precipitation region. According to the "calibration" of CNA by the concurrent measurements of electrons of different energies, the maximum effect on CNA is expected from 30- to 150-keV electrons [*Collis and Korth*, 1985]. The corresponding threshold rigidities are 600 and 1400 nT km, respectively.

The pattern of Figure 4 and the regular rigidity dependence of IB position are naturally explained by the precipitation originating from weak nonadiabatic effects (pitch

TABLE 1. Corrected Geomagnetic Coordinates Calculated for Points in the Ionosphere at 110 km Altitude Above the Riometers and Balloons During Growth Phases of Substorms on May 23, 1979, and June 23, 1979

Station or Balloon	Abbreviation	Corrected Geomagnetic Latitude, deg	Corrected Geomagnetic Longitude, deg	May 23, 1979			June 23, 1979		
				Onset Time, UT	Maximum Precipitation Time, UT	Maximum CNA, dB	Onset Time, UT	Maximum Precipitation Time, UT	Maximum CNA, dB
KA0622	K22	69.7	87.7				1945	1950	weak X ray peak
Dixon	DIX	67.75	155.7						
Andoya	AND	66.31	102.6					2023	1.7
Kevo	KEV	66.00	111.2	1920	1945	0.9	2000	2027	1.0
Leirvogour	LEI	66.00	69.5	1942	2012	0.8	2022	2040	0.5
S00622	S22	65.64	93.1				2010	2036	intense X ray peak
Ivalo	IVA	64.83	110.5	1945	2003	1.7	2025	2047	1.4
Ugorskiy Shar	USH	64.48	137.7	1940	2000	1.7	2020	2040–2050	1.2
Sodankylä*	SOD	63.73	108.9				2045		
S00623*	S23	63.44	109.5				2055		

The onset and maximum precipitation times and the maximum CNA magnitudes are also shown. The peak intensity of auroral X rays of energy in excess of 25 keV, as observed by the balloon S22 on June 23, 1979, was about 20 times the background [*Tanskanen et al.*, 1987]. No CNAs were observed either on May 23, 1979, or on June 23, 1979, for Dixon.

*For May 23, 1979, no CNA was observed until the expansion onset. For June 23, 1979, CNA was observed growing up to the expansion onset.

angle diffusion) occurring in the equatorial current sheet. These effects have been extensively studied today [*Gray and Lee*, 1982], particularly with applications to particles mirroring near the ionosphere [*Sergeev et al.*, 1983; *Sergeev and Malkov*, 1988]. According to the latter results the IB position in the ionosphere is expected on those flux tubes which meet the following condition in the central plane of the equatorial current sheet:

$$K_c \equiv R_c/\rho = \left(B_z^2 \Big/ G \frac{\partial B_x}{\partial z} \right) \quad (1)$$

All the field components here refer to a local coordinate system where z is perpendicular to the current sheet, x is determined by the magnetic field outside (above) the current sheet, and y completes the system. R_c is the field line curvature radius at the equator, and $\rho = G/B_z$. K_c is about 8 for the given range of rigidities (of the order of 1000 nT km). This mechanism was shown by *West et al.* [1978], *Sergeev et al.* [1983], and *Sergeev and Malkov* [1988] to explain the real IB position for particles of different rigidities.

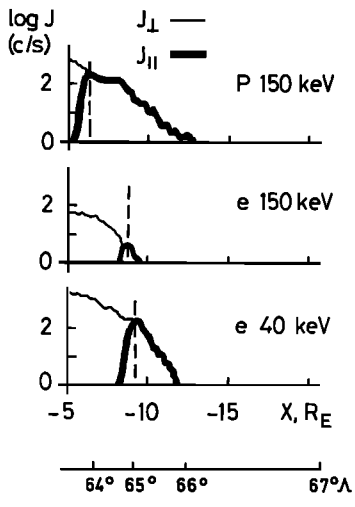

Fig. 4. A schematic presentation of the main features of the fluxes of precipitated ($J_\parallel$, in the center of the loss cone) and trapped ($J_\perp$, outside the loss cone) energetic protons (p) and electrons (e) in the nightside magnetosphere. The relationship between the invariant latitude Λ and the equatorial x values corresponds approximately to the epoch at 2010 UT on May 23, 1979.

From (1) it is found that during the growth phase, the expected decrease of the current layer thickness and the observed decrease of B_z in the near-tail region will move the IB position inside the radiation belt. As the field lines are stretched, the latitude of the ionospheric projection of a fixed point in the magnetosphere decreases. Both effects give rise to the equatorward drift of the precipitation region. According to the discussion given above, we may interpret the maximum amplitude of CNA (or X ray) amplitude as a signature of IB position of energetic electrons over the riometer (or balloon). This implies that (1) is satisfied at that time in the corresponding flux tube close to the equator. The application of this method to evaluate the variable parameters of the current sheet obviously requires additional information about magnetic field line configuration outside the current sheet at this particular moment.

4. Modeling the Magnetic Configuration

An accurate model of the whole nightside magnetosphere at any particular time would require many simultaneous measurements of fields and currents in space. However, our task is simpler, since the field model and, accordingly, measurements are needed only in a limited region: within 10–12 R_E distance in the narrow MLT sector, conjugate to northern Scandinavia. On May 23, 1979, the spacecraft configuration was favorable for such measurements (Figure 1). ISEE 1 was about 3 R_E below the expected position of the center of the current sheet and could be used to monitor the integral intensity of the current in the near-Earth tail. At the same time a smooth interpolation of the external B_z field values, measured by GEOS 2 and ISEE 1, will yield the field line inclination in the region of interest.

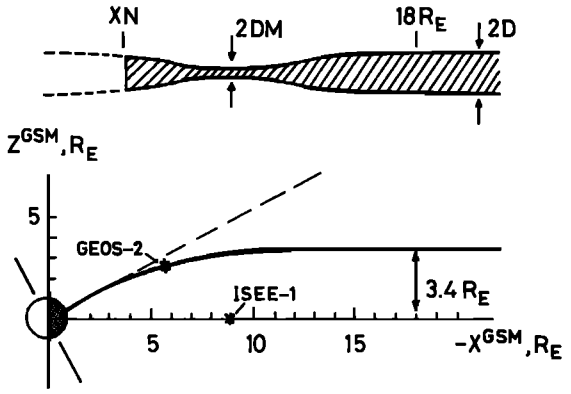

Fig. 5. (Top) Configuration of the current sheet thickness and (bottom) the geometry of the curved current sheet plane used in model calculations.

As a basis for our modeling we use the magnetic field presentation employed by *Tsyganenko* [1987], hereafter referred to as the T87 model. The sources of the external (dipole field subtracted) field $\Delta\mathbf{B}$ are presented here in the following form:

$$\Delta\mathbf{B}(r) = \mathbf{B}_{DCF} + \mathbf{B}_{DR}(DR, \rho_0) + f\mathbf{B}_T(J^{Kp}(x), XN, D, DM) \quad (2)$$

The effects of the currents at the dayside magnetopause (*DCF*) plus all other effects not included in the ring current (*DR*) and tail current (*T*) contributions, were represented by polynomial expansions and have been determined from the extensive experimental data set in T87. They are retained in the term B_{DCF}. The two parameters describing the *DR* contribution are the radius of *DR* current (ρ_0) and the ring current field intensity (*DR*), which was adjusted to the conditions of that day. Using the D_{st} value of -18 nT plus a correction for the solar wind dynamic pressure in the form $DR/\text{nT} = D_{st}/\text{nT} - 0.024V(n)^{1/2}$, where n (cm^{-3}) and V (kilometers per second) are the solar wind density and velocity, respectively, we estimate that $DR \approx -40$ nT.

The tail currents in T87 are the plasma sheet current plus its closure currents at the magnetopause. The sheet current has been represented as a superposition of finite size current filaments having an intensity decreasing monotonously with distance from the Earth. These radial profiles of linear current density $J^{Kp}(x)$ have been determined in T87 for a few groups of activity levels (parametrized by *Kp* index). They are retained in our approach. However, by multiplying $\mathbf{B}_T$ in (2) by an arbitrary factor f, we allow for the change of the total tail current.

The main modifications of the T87 model in our case concern the geometry of the plasma sheet current in the near-tail region. First, we introduce the inhomogeneous thinning of the sheet current (see Figure 5) in the form

$$D(x) = 0.5 * (D + DM + (D - DM) * \cos[2\pi * (x/18 + 1)])$$

The position of the (first) minimum half thickness (*DM*) was fixed at $x = -9\,R_E$. The half thickness smoothly increases to its maximum value D at $x = -18\,R_E$ and remains constant at larger distances. The pattern of this inhomogeneous thinning was chosen following the results of *Nishida and Fujii* [1976].

The second modification concerns the geometry of the "neutral sheet" (center plane of the current sheet near midnight). Taking into account that the neutral sheet smoothly joins the magnetic equator at $r \le 4\,R_E$ [*Fairfield et al.*, 1987] and that the height of the neutral sheet from the equatorial plane at $x \le -10\,R_E$ is about $7.5\,R_E * \sin\Psi$ [*West et al.*, 1978], where Ψ is the angle of dipole tilt to the Sun, then for the particular time at 2010 UT on May 23, 1979, we have approximated the neutral sheet surface at $x \ge -11.74$ R_E as one half of the parabola:

$$z = 3.4 - 0.0247(x + 11.74)^2$$

which smoothly merges into the plane current sheet at further distance (see Figure 5). In this geometry, GEOS 2 is located close to the neutral sheet surface, in agreement with magnetic observations. The inner edge position (*XN*) of the current sheet is one more parameter to be determined.

This model was adopted as a numerical algorithm to calculate the magnetic field at an arbitrary point using the free parameters, f, *XN*, *D*, and *DM*. Different profiles of tail current density $J^{Kp}(x)$ of the T87 model were applied, and the ring current term *DR* was varied from -35 to -45 nT. A set of field models was identified giving a fit within 1–2 nT of the observed values of B_z at both spacecraft and of B_x at ISEE 1. A few representative variants are given in Table 2. It is to be noted that no attempt was made to reproduce accurately the B_x component at GEOS 2, since in a chosen

TABLE 2. The GSM Components of the External (Dipole Field Subtracted) Magnetic Field During the Growth Phase of the Substorm on May 23, 1979, Measured by GEOS 2 and ISEE 1 Spacecraft and Calculated for a Few Best Fits of the Tsyganenko Model Corresponding to Different *DM* Values

	GEOS 2			ISEE 1			Model*					
Time, UT	B_x	B_y	B_z	B_x	B_y	B_z	*Kp*	f	*XN*	*DR*	*D*	*DM*
2010	−12.	+8.	−41.6†	−39.0	7.2	−16.0†						
	−8.7	−1.4	−42.2	−39.5	0.1	−17.0	3	1.7	−2.8	−45.	1.	0.1
	−8.6	−1.4	−41.7	−39.4	0.1	−17.0	3	1.7	−2.8	−45.	1.	0.2
	−8.4	−1.4	−40.8	−39.2	0.1	−17.0	3	1.7	−2.8	−45.	1.	0.4
	−8.8	−1.4	−39.5	−39.4	0.1	−17.7	3	1.75	−2.8	−45.	1.	1.
1945	−8.	+7.	−33.6†	−32.5†	4.6	−13.2						
	0.4	−2.1	−35.4	−32.9	−0.5	−11.5	3	1.5	−2.4	−35.	1.	0.1
1830	−2.	+9.	−23†	−18.3†	3.0	−6.8†						
	1.6	−4.2	−24.3	−17.1	−0.4	−7.2	3	1.0	−3.7	−40.	2.07	2.0

*No entry means that the magnetic field values in the same line are measured, not modeled values.
†Measured values of the magnetic field that were fitted by the model calculations.

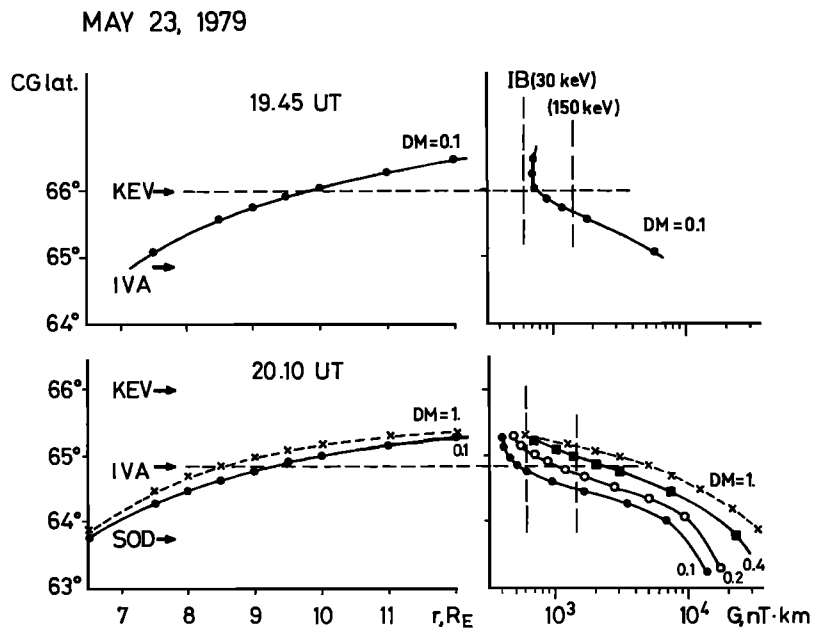

Fig. 6. Correspondence (left) between ionospheric and equatorial positions of flux tubes at 110° CG longitude magnetic meridian and (right) between latitude and critical IB rigidities for a few representative magnetic field models given in Table 2.

fixed neutral sheet geometry with a thin current, this component is very sensitive to small variations in spacecraft position relative to the neutral sheet. Nevertheless, the correspondence between the calculated and the measured values is fairly good. Further, there are systematic discrepancies between the B_y values of the model and those of the observations. These can be attributed to the effects of field-aligned currents. These discrepancies do not significantly influence our results, since they only affect the longitude of the ionospheric projection but not the latitude which is of main interest in the current study. When applying different J^{Kp} profiles of T87, we found a reasonable agreement between the model and the observations only for Kp = 3. Note also the low sensitivity of the modeled magnetic field at the spacecraft positions to the minimum current sheet thickness (DM), documented by the various fits in Table 2.

5. Estimate of the Current Sheet Thickness and Evolution of the Magnetic Configuration During Growth Phase

Let us first consider the situation at 2010 UT on May 23, 1979, i.e., 8 min before the expansion onset and 7 min after the maximum CNA values at Ivalo. For all selected models we calculated the configuration of magnetic field lines anchored in the ionosphere along the 110° corrected geomagnetic (CG) longitude magnetic meridian (see Figure 6). The results of our calculations indicate that the latitudes of the ionospheric projections of fixed magnetospheric points agree to within 0.2° CG latitude. The projection of the ionospheric point above Ivalo to the current sheet falls at $r = (9.0 \pm 0.5)$ R_E in all cases. On the other hand, the corresponding latitude versus rigidity profiles, as calculated from (1), are very dependent on the current sheet thickness. From Figure 6 it can also be seen that if the IB position of 30-keV electrons is to be projected to (or southward of) Ivalo, the current sheet thickness is not more than 0.1 R_E. The energetic electron precipitation data is seen to be very sensitive to the current sheet thickness. This is so, provided our interpretation of the origin of the precipitation is correct. Let us now briefly discuss the various sources of possible errors for the above estimates.

Errors in the Mapping

From numerical experiments with the model, changes of 0.2°–0.3° CG latitude for ionospheric projections were found, as well as a displacement of less than 1 R_E for the magnetospheric projections of fixed ionospheric points, when changing B_z by 2 nT inside a region of 6–10 R_E. Since our fits to the observations are within 1 nT (Table 2), these errors seem insignificant.

As was pointed out earlier, systematic differences between the observed and the modeled values of B_y are evident, because effects caused by B_y were not included in the modeling. However, offsets in B_y of the order of 10 nT will result in a longitudinal displacement of only a few degrees for the calculated ionospheric projection. As a result of the very small slope of the precipitation region with respect to the lines of constant CG latitude (only 0.35°–0.45° of CG latitude per 15° of CG longitude; see Figure 3), this will not significantly affect the results.

Errors Due to the Finite Size of the Antenna Cone of Riometers

If the precipitation region does not completely fill the riometer antenna pattern, the CNA amplitude is reduced considerably. When, for example, only one half of a riometer antenna pattern is "filled" with maximum cosmic noise absorption, the registered CNA value is only 3 dB. For this reason the maximum CNA amplitudes are expected when, during its equatorward motion, the sharp IB reaches the southern limit of the antenna cone rather than the zenith of the station. The cone half width of a Finnish riometer is

about 0.3° CG latitude along the meridian [*Ranta and Ranta*, 1978], so the real IB position at the meridian may be 0.3° lower than the one used in the comparison. The very accurate determination of IB position, however, requires the knowledge of the real IB thickness which may be of the same magnitude. Furthermore, this effect can only reduce the *DM* values.

Errors Due to Inaccurate Model of the External Field Close to the Current Sheet

The real current distribution may be more complicated than the one used in the model. Thus the real field inclination and the equatorial distance from fixed ionospheric field lines may differ from our results. The most serious case is that in which the true B_z component close to the current sheet is depressed relative to its model value, interpolated from GEOS 2 and ISEE 1 observations. According to (1) this may move the equatorial IB position outward of the modeled region (10–12 R_E) and seriously affect our estimates. The recent results from a statistical survey of the magnetic field out to 8.8 R_E [*Fairfield et al.*, 1987] allow for a twofold evaluation of the situation. First, within 0.5 R_E of the current sheet center at $r \approx 8.5$–8.8 R_E the real B_z values range from 11 to 27 nT, with very few 1-min resolution points below 10 nT during 48 hours of observations. We take 10 nT to be the lower limit for B_z at $r \approx 9$ R_E during the growth phase for both of the studied cases. In our model the B_z values are only slightly higher ($B_z = 15$ nT) in the corresponding region. From simple geometrical arguments it seems clear that when replacing $B_z = 15$ nT by $B_z = 10$ nT, while keeping $B_x = 40$ nT fixed, the change of field inclination is not large and will not significantly distort the field line. Assuming the half thickness of the region where B_z is depressed with respect to the model adjusted values to be about 1 R_E, the upper limit of the outward displacement of the field line at the equator will be 1.5 R_E. Note that the real field was measured by ISEE 1 to be only 3 R_E below the current sheet at a similar radial distance. If the current sheet is thicker than a few tenths of R_E, the effects are reduced. On the other hand, decreasing B_z will change the estimated D values. Scaling in (1) as

$$D_{\max} = D_{\text{obs}}(B_z^{\text{obs}}/B_z^{\min})^2$$

and substituting $B_z^{\text{obs}} = 15$ nT and $B_z^{\min} = 10$ nT will yield $D_{\max} \approx 2D_{\text{obs}} \approx 0.2$ R_E.

These exercises indicate that the calculated estimates of the current sheet thickness are accurate to within a factor of 2 and that the equatorial position of the isotropic boundary of 40-keV electrons at the end of the growth phase is inside a distance of 10 R_E. The field line configurations at the beginning and end of the growth phase on May 23 are drawn in Figure 7. The ionospheric projection of the GEOS 2 spacecraft was all the time to the south Sodankylä, well to the south of the CNA band.

During the growth phase of the substorm on May 23, 1979, at the time of the CNA maximum at Kevo (1945 UT), the best fit between spacecraft and ground-based observations was found for DM = 0.1 R_E. The corresponding equatorial IB position, projected from the ionospheric point over Kevo, was at $r = 9.8$ R_E (see Table 2 and Figure 6). Note from Figure 6 that the change in the CNA meridional position between 1945 and 2010 UT is mainly (up to 80%) due to the change in magnetic configuration.

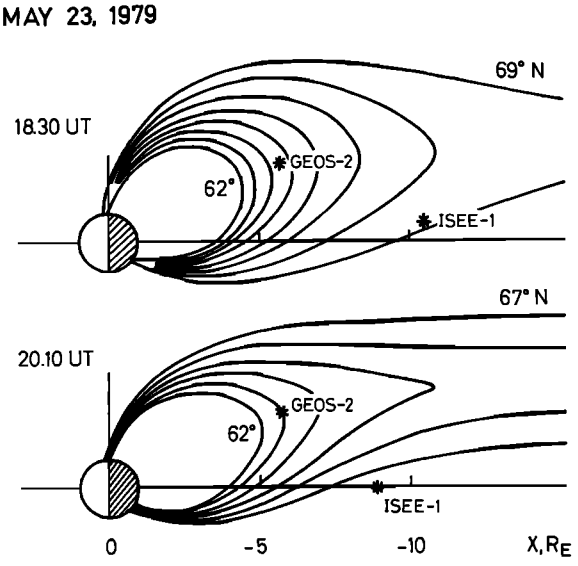

Fig. 7. Magnetic field configurations in the midnight meridional plane at the beginning and at the end of the growth phase of the May 23, 1979, substorm.

According to the T87 model the average equatorial IB position for 40-keV electrons at the onset of the substorm growth phase (1830 UT) is at $r = 18$ R_E and about 69° CG latitude in the midnight sector. This position is just outside the outer boundary of the pseudotrapping region, calculated from the model as the outer drift shell of particles mirroring near the ionosphere. According to the discussions of *Sergeev and Tsyganenko* [1982] this region cannot contain measurable fluxes of energetic electrons in quiet conditions. For the same reason we do not expect to see any measurable CNA at stations like Dixon, which was located slightly to the south of the estimated ionospheric projection of the IB at the beginning of the growth phase but showed no measurable effects until the expansion phase (Table 1).

6. Discussion

This study presents to our knowledge the first attempt to model quantitatively the evolution of the magnetic tail during the growth phase of an individual substorm. The model uses a realistic presentation for the tail current, taking into account the curved form and the inhomogeneous thinning of the current sheet in the near-Earth region. The model parameters are adjusted to reproduce the magnetic field observed by two spacecraft in the near-tail region. Since the measurements and results concern a small region of the magnetosphere covered by observations at a distance of 6–10 R_E within 2200–2300 MLT, caution is necessary when expanding the results to cover the whole tail. *Nishida and Nagayama* [1973] have reported that the tail lobe field rarely increases by more than 30% during the growth phase, in agreement with the IMP-J data given in Table 2. In our event of May 23 the estimated increase is 70%. The discrepancy may be regarded as an indication of a stronger increase in the near-Earth domain of the tail current.

The only quantitative indication of a very intense thinning

comes from observations of a fast-thinning wave which flattens the gyrocenters of energetic ions into a layer which is about 0.1 R_E thick [*Buck et al.*, 1973]. These observations have been made at the end of an intense growth phase at $r \approx 8\ R_E$ and within 1 R_E of the estimated position of the neutral sheet. The total magnetic tail field was in excess of 60 nT. An energetic electron precipitation peak was detected by balloon X ray measurements of 65° CG latitude. The isotropization of the pitch angle distribution of energetic electrons without any accompanying increase in wave activity was documented at OGO 5 and reported by *West et al.* [1973]. Unfortunately, the equatorial distance to the innermost flux tube containing isotropic electrons (IB) cannot be estimated in this case. The mechanism of the current sheet scattering of energetic electrons was first invoked on the basis of these observations, which agree in all main features with our results.

Important support to this particle-scattering mechanism is presented by *West et al.* [1978]. By applying a magnetic field model based on in situ measurements on board the OGO 5 spacecraft, they were able to compare the calculated and observed position of an isotropic boundary and found an excellent agreement between them. Although their results correspond to low-activity periods without strong substorms, in one case (August 2, 1968) they found the 1-R_E half thickness for the current sheet and the 11-R_E distance for IB of 80-keV electrons at the equator.

Takahashi et al. [1978] have reported on observations made by Active Magnetosphere Particle Tracer Explorers/CCE of a disruption of the magnetotail at a radial distance of about 8 R_E in the midnight sector at the onset of a substorm. This may have resulted from a near-Earth thinning of the current sheet and the formation of a neutral line. They also showed evidence for what could be interpreted as the motion of this region. Unfortunately, their observations from only one spacecraft did not allow for an estimation of the current sheet thickness.

Indirect evidence of a strong thinning of the near-Earth current sheet is also provided by the observations of complete energetic particle dropouts, which are typical for a growth phase at $r \approx 6$–$8\ R_E$ [*Feynman et al.*, 1984]. They have also been observed at those geosynchronous satellites, for example, ATS 6, which are about 1 R_E above (or below) the geomagnetic equator. An important distinction between the energetic particle dropouts, apparently produced by the current sheet thinning, and the plasma sheet thinning is that the auroral (keV) plasma occupies spatially a more extended region [*Feynman et al.*, 1984]. A good illustration of this statement is seen in the ISEE 1 data for the event on May 23, 1979. The very strong increase in the B_x component on board ISEE 1 (Figure 1) gives an impression that ISEE 1 was well outside the current sheet. At the same time the 6-keV proton flux measured by ISEE 1 (not shown here) did not fall below 10^6 (keV cm^2 s sr)$^{-1}$, i.e., the spacecraft stayed within the plasma sheet during the whole period.

Strong evidence has been given here in support of the inferred thin current sheet configuration as well as of the particle-scattering mechanism. At the same time, other alternative explanations to the observed precipitation pattern have been discussed in the literature. The first one [*Tanskanen et al.*, 1987, and references therein] includes the acceleration of energetic electrons or their precipitation into the ionosphere through a Fermilike acceleration process by a large-scale electric field. However, this acceleration provides the precipitation only near the loss cone boundary and thus cannot explain the isotropic distributions of the precipitated particles documented by *Rossberg* [1976]. The second hypothesis connects the precipitation band in an unspecified way to the inner edge of the plasma sheet or the injection boundary [*Tanskanen et al.*, 1987]. Referring to the close similarity between the two growth phase cases (May 23, 1979, and June 23, 1979) and to the appearance of the inner edge of the plasma sheet in the proximity of GEOS 2 at the end of the growth phase on June 23, 1979 [*Tanskanen et al.*, 1987], we note that the GEOS 2 ionospheric projection falls 0.3° CG latitude below the corrected geomagnetic latitude of Sodankylä, where no significant CNA is yet seen. Thus the projections in our model, which are not sensitive to the particular choice of the current sheet thickness, indicate that the maximum energetic electron precipitation originates in the flux tubes located at the equator, a few R_E tailward of GEOS 2 and thus tailward of the inner edge of the plasma sheet. Hence these two alternative interpretations clearly disagree with the available experimental information.

Further evidence in favor of the mechanism of energetic electron precipitation that was used comes from its ability to provide a consistent explanation to the main known morphological features of this precipitation, to be discussed below.

Configuration and Width of the Precipitation Region

A typical convexlike form of CNA region, well documented by *Ranta et al.* [1981], *Tanskanen et al.* [1987], and Figure 3, is naturally explained by the model. Some quantitative differences between the inclination of this curve and the experimental lines may be prescribed to the azimuthal inhomogeneity of the thinning process which cannot be modeled properly using the available data set.

According to the discussion by *Sergeev and Tsyganenko* [1982] the outer boundary of the radiation belt during a quiet period is expected at 12–15 R_E. This is due to large drift losses of energetic particles outside this region. Together with the position of the isotropic boundary at 9–10 R_E this explains the 1°–2° CG latitude meridional width of the precipitation belt (see Figure 4), well documented by our study and previous studies.

Intensity Variations

According to *Ranta et al.* [1981], *Tanskanen et al.* [1987], and data in Figures 1 and 2 and Table 1, the intensity of CNA in the center of an equatorward moving CNA band displays an evident increase during the growth phase. The inward IB motion toward flux tubes containing higher particle fluxes offers a natural explanation to this feature.

Drift Speed

The drift speeds of CNA bands in Figures 1–3 are very typical [*Ranta et al.*, 1981]. The model presented conclusively shows that the temporal evolution of the magnetic field during the growth phase is the main cause for the observed equatorward motion of the precipitation region. It is important to note that approximately 80% (1° CG latitude) of the meridional displacement from Kevo to Ivalo between 1945 and 2003 UT on May 23, 1979, is due to the tailward

stretching of the field lines while the remaining 20% (0.1°–0.3° CG latitude) is due to the earthward motion of the source region (from 9.8 to 9.2 R_E at the equator; see Figure 6).

Variations of the Energy Spectrum

A hard auroral X ray spectrum at the beginning of an event as recorded by balloons, followed by the steadily softening spectrum during the maximum stage and at the end of the precipitation event [*Tanskanen et al.*, 1987], can be explained by the rigidity dependence of the IB position. According to Figure 6 the region between isotropic boundaries of 30-keV and 150-keV electrons, i.e., the region of hard precipitation, is expected to have a 0.3°–0.4° CG latitude width along the meridian. With the estimated average CNA drift speed (0.06°–0.07° min^{-1}) the transition time between hard and soft precipitation in the beginning of the bay is expected to be 5–8 min, which is close to the duration of this phase observed on June 23, 1979.

Another significant spectral variation, the progressive hardening of the energy spectra in the course of the growth phase [*Tanskanen et al.*, 1987], reflects the softening of the energy spectrum of energetic electrons when moving toward the outer edge of the radiation belt [*McDiarmid and Hruska*, 1972]. The obvious reason for such a spectral variation of the radiation belt electrons is the faster drift cone loss of the more energetic particles in the pseudotrapping region [*Sergeev and Tsyganenko*, 1982].

Thus the good ability of the IB model to explain all the main morphological features of the energetic electron precipitation during the growth phase strongly supports the interpretation and gives more confidence to using these precipitated particles as tracers of the configuration of the equatorial current sheet.

In the following discussion an evaluation is presented of the theoretical predictions by *Büchner and Zelenyi* [1987] on the time and location of the explosive growth of the tearing mode instability, corresponding, in their picture, to the transition from the substorm growth to the expansion phase. Their mechanism requires chaotization of the motion of thermal electrons in the current sheet with small B_z or possibly with a very small thickness. According to *Büchner and Zelenyi* [1987], using a lobe field value of 40 nT, a current sheet half thickness of 0.1 R_E, and an electron temperature of 1 keV, the threshold value for the instability onset to occur is B_z = 4 nT. In the model calculations presented in this paper such small threshold values of B_z would hardly occur at distances of $r \leq 9$–$10\ R_E$. Nevertheless, they are likely to exist slightly further out in the tail. Thus the results obtained indicate that the current sheet in the nightside magnetotail at the end of a growth phase is reasonably close to being unstable against the tearing mode instability at $r \geq 10\ R_E$, as described by *Büchner and Zelenyi* [1987].

7. Conclusions

The results presented illustrate in a quantitative manner the time evolution of the magnetic configuration in the night sector of the near-Earth tail during the substorm growth phase. This evolution seems to be the main factor leading to the well-known equatorward expansion of the auroral oval. It was estimated that about 80% of this equatorward expansion is due to the time variation of the magnetic configuration.

By interpreting the observed precipitation of energetic electrons in terms of particle pitch angle diffusion in the equatorial current sheet, we were able to estimate the current sheet half thickness at the end of the growth phase. This half thickness has to be very small, about 0.1 R_E at $r \approx 9\ R_E$, in order explain the energetic electron precipitation by the proposed mechanism. It is suggested that the flattened current sheet at $r \approx 10\ R_E$ is embedded within a broad (a few R_E) plasma sheet.

Acknowledgments. The ISEE 1 data pool tapes and magnetic data of IMP-J spacecraft have been provided through WDC-A (R and S) by courtesy of J. I. Vette. We are grateful to H. Ranta and A. Ranta (Sodankylä observatory, Finland), T. Saemundsson (Science Institute, University of Iceland), and O. Troshichev (Arctic and Antarctic Research Institute, USSR), who kindly provided us with the riometer charts. We thank N. Tsyganenko for instructive discussions and for the opportunity to use some of his computer subroutines. The assistance of L. L. Nemtseva and M. V. Holeva in the preparation of the figures and manuscript is gratefully acknowledged. The work by three of us (V.A.S., P.T., and K.M.) was supported through the Soviet-Finnish working groups on geophysics and space research. P.T. and K.M. also acknowledge the financial support of the Academy of Finland.

The Editor thanks A. S. Rodger and L. J. Zanetti for their assistance in evaluating this paper.

References

Büchner, J., and L. M. Zelenyi, Chaotization of the electron motion as the cause of an internal magnetotail instability and substorm onset, *J. Geophys. Res.*, *92*, 13,456, 1987.

Buck, R. M., H. I. West, and R. G. D. D'Arcy, Satellite studies on magnetospheric substorms on August 15, 1968, 7, OGO 5 energetic proton observations: Spatial boundaries, *J. Geophys. Res.*, *78*, 3103, 1973.

Collis, P. N., and A. Korth, GEOS-2 observations of energetic electrons in the morning sector during auroral radio absorption events, *J. Atmos. Terr. Phys.*, *47*, 327, 1985.

Fairfield, D. H., R. P. Lepping, E. W. Hones, S. J. Bame, and J. R. Asbridge, Simultaneous measurements of magnetotail dynamics by IMP spacecraft, *J. Geophys. Res.*, *86*, 1396, 1981.

Fairfield, D. H., M. H. Acuna, L. J. Zanetti, and T. A. Potemra, The magnetic field of the equatorial magnetotail: AMPTE CCE observations at $R < 8.8\ R_E$, *J. Geophys. Res.*, *92*, 7432, 1987.

Feynman, J., D. A. Hardy, and E. G. Mullen, The 40-keV electron durable trapping region, *J. Geophys. Res.*, *89*, 1517, 1984.

Fritz, T. A., Study of the high-latitude, outer-zone boundary region for ≥40 keV electrons with satellite INJUN 3, *J. Geophys. Res.*, *75*, 5387, 1970.

Gray, P. C., and L. C. Lee, Particle pitch angle diffusion due to nonadiabatic effects in the plasma sheet, *J. Geophys. Res.*, *87*, 7445, 1982.

Imhof, W. L., J. B. Reagan, and E. E. Gaines, Studies of the sharply defined L dependent energy threshold for isotropy at the midnight trapping boundary, *J. Geophys. Res.*, *84*, 6371, 1979.

King, J. H., Interplanetary medium data book, supplement 3A, *Rep. NSSDC/WDC-A-86-04A*, Natl. Space Sci. Data Cent., Greenbelt, Md., April 1986.

Lester, M., W. J. Hughes, and H. J. Singer, Polarization patterns of Pi 2 magnetic pulsations and the substorm current wedge, *J. Geophys. Res.*, *88*, 7958, 1983.

Lundblad, J. A., F. Søraas, and K. Aarsnes, Substorm morphology of >100 keV protons, *Planet. Space Sci.*, *27*, 841, 1979.

McDiarmid, J. B., and A. Hruska, Anisotropy of high-latitude electron fluxes during substorms and structure of the magnetotail, *J. Geophys. Res.*, *77*, 3377, 1972.

McPherron, R. L., A. Nishida, and C. T. Russell, Is near-Earth current sheet thinning the cause of auroral substorm onset?, in *Quantitative Modelling of Magnetosphere-Ionosphere Coupling*

Processes, edited by Y. Kamide and R. A. Wolf, p. 252, Kyoto Sangyo University, Kyoto, Japan, 1987.

Nishida, A., and K. Fujii, Thinning of the near-Earth (10–15 R_E) plasma sheet preceding the substorm expansion phase, *Planet. Space Sci.*, *24*, 849, 1976.

Nishida, A., and N. Nagayama, Synoptic survey for the neutral line in the magnetotail during the substorm expansion phase, *J. Geophys. Res.*, *78*, 3782, 1973.

Ranta, H., and A. Ranta, Riometer measurements of ionospheric radio wave absorption, *J. Atmos. Terr. Phys.*, *40*, 799, 1978.

Ranta, H., A. Ranta, P. N. Collis, and J. K. Hargreaves, Development of the auroral absorption substorm: Studies of pre-onset phase and sharp onset using an extensive riometer network, *Planet. Space Sci.*, *32*, 1287, 1981.

Rossberg, L., Prebay electron precipitation as seen by balloons and satellites, *J. Geophys. Res.*, *81*, 3437, 1976.

Russell, C. T., and R. L. McPherron, Magnetotail and substorms, *Space Sci. Rev.*, *15*, 205, 1973.

Schindler, K., and J. Birn, Self-consistent theory of time dependent convection in the Earth's magnetotail, *J. Geophys. Res.*, *87*, 2263, 1982.

Sergeev, V. A., and M. V. Malkov, On diagnostics of tail magnetic configuration (in Russian), *Geomagn. Aeron.*, *4*, 649, 1988.

Sergeev, V. A., and N. A. Tsyganenko, Energetic particle losses and trapping boundaries as deduced from calculations with a realistic magnetic field model, *Planet. Space Sci.*, *30*, 999, 1982.

Sergeev, V. A., E. M. Sazhina, N. A. Tsyganenko, J. A. Lundblad, and F. Søraas, Pitch-angle scattering of energetic protons in the magnetotail current sheet as the dominant source of their isotropic precipitation into the nightside ionosphere, *Planet. Space Sci.*, *31*, 1147, 1983.

Singer, H. J., W. J. Hughes, P. F. Fougere, and D. J. Knecht, The localization of Pi 2 pulsations: Ground-satellite observations, *J. Geophys. Res.*, *88*, 7029, 1983.

Takahashi, K., L. J. Zanetti, R. E. Lopez, R. W. McEntire, T. A. Potemra, and K. Yumoto, Disruption of the magnetotail current sheet observed by AMPTE/CCE, *Geophys. Res. Lett.*, *14*, 1019, 1987.

Tanskanen, P., et al., Different phases of a magnetospheric substorm on June 23, 1979, *J. Geophys. Res.*, *92*, 7443, 1987.

Tsyganenko, N. A., Global quantitative models of the geomagnetic field in the cislunar magnetosphere for different disturbance levels, *Planet. Space Sci.*, *35*, 1347, 1987.

West, H. I., R. M. Buck, and J. R. Walton, Satellite studies of magnetospheric substorms on August 15, 1968, 6, OGO 5 energetic electron observations: Pitch angle distributions in the nighttime magnetosphere, *J. Geophys. Res.*, *78*, 3093, 1973.

West, H. I., R. M. Buck, and M. G. Kivelson, On the configuration of the magnetotail near midnight during quiet and weakly disturbed periods: Magnetic field modeling, *J. Geophys. Res.*, *83*, 3819, 1978.

R. C. Elphic, Los Alamos National Laboratory, MS D438 Los Alamos, NM 87545.

A. Korth, Max-Planck-Institut für Aeronomie, D-3411 Katlenburg-Lindau 3, Federal Republic of Germany.

K. Mursula and P. Tanskanen, Department of Physics, University of Oulu, Linnanmaa, SF-90570 Oulu 57, Finland.

V. A. Sergeev, Institute of Physics, Leningrad State University, Leningrad 198904, USSR.

(Received March 10, 1989;
revised July 25, 1989;
accepted August 14, 1989.)